Qualitative analysis of a 3D multiphysics model for nonlinear ultrasonics and vibration induced heating at closed defects

Kevin Truyaert, Vladislav Aleshin, Koen van den Abeele

Article

Qualitative analysis of a 3D multiphysics model for nonlinear ultrasonics and vibration induced heating at closed defects

Kevin Truyaert[1,*], Vladislav Aleshin [2,3] and Koen Van Den Abeele [1]

[1] KU Leuven campus Kulak, B-8500 Kortrijk, Belgium
[2] Univ. Lille, CNRS, Centrale Lille, ISEN, Univ. Valenciennes, UMR 8520–IEMN, LIA LICS/LEMAC, F-59000 Lille, France
[3] Tomsk State University, 634050 Tomsk, Russia
* Correspondence: kevin.truyaert@kuleuven.be

Abstract: Upon exciting a material using elastic waves, the locally induced deformation at the interfaces of internally closed defects may cause nonlinear wave mechanics and dynamics in the form of clapping and friction. As a result, both phenomena instigate spectral broadening of the excitation spectrum as well as the production of heat, directly originating from the defect. To better understand and account for the physics behind the dissipation of energy by internally closed defects as a result of the wave-interface interaction, dedicated models can be developed. In this work, we propose a 3D finite element multiphysics model that is capable of simultaneously describing the generation of nonlinearities and heating at a defect's interface experiencing clapping and friction induced by elastic wave propagation. The model consists of three different modules. The first module describes the elastic wave propagation in a virgin/bulk material, whereas the second module captures the contact physics at the defect level. The third module is implemented to calculate the diffusion of thermal energy in the specimen. The contact physics module accounts for anharmonic and hysteretic effects, describing the nonlinear behavior of the defect's interfaces, which is echoed in both the ultrasound spectrum and in the vibration induced heating. A qualitative analysis of the computational model, integrating the three modules, is performed to validate the approach. Examples show that nonlinear spectral components are indeed observed as a result of the friction and the clapping experienced by the faces of the defect. At the same time, a localized temperature increase due to the induced friction is noted, and its response at the outer surface of the sample is examined. The qualitative validation approves that the model is ready to be tested further quantitively, and to compare its predictions to experiments.

Keywords: Ultrasound; Modelling; Friction

Citation: Truyaert, K.; Aleshin, V.; Van Den Abeele, K. Qualitative analysis of a 3D multiphysics model for nonlinear ultrasonics and vibration induced heating at closed defects. *Journal Not Specified* **2021**, *1*, 0. https://doi.org/

Received:
Accepted:
Published:

1. Introduction

Ultrasonic vibrothermography is an auspicious Non-Destructive Testing (NDT) technique for the detection of closed defects, either fully internal or surface breaking. The principle of ultrasonic vibrothermography is simple: through excitation by ultrasonic waves, frictional behavior at the defect's interfaces takes place. As a result, the vibrational energy of the elastic wave will locally be converted into thermal energy, generating heat around the defect, which subsequently dissipates through the medium by way of thermal diffusion. In practice, the distributed heat can be recorded by an infrared camera, possibly detecting the heat signature and its origin. Next to defect detection, defect characterization has become one of the major research interests in NDT, in particular to anticipate the severity of the defect. However, to obtain reliable and high quality defect classification by ultrasonic thermography, theoretical models capable of interpreting the obtained thermograms are necessary.

Contact models come in all shapes and sizes. Some models only take into account clapping (the normal behavior) [1], but more realistic models also include friction (the tangential behavior). The contact profile of the two bodies in contact also greatly influences the response of the applied loading procedure. Some studies assume the bodies in

contact to have flat faces [2] whereas other models introduce non-flat surface, allowing to account for roughness [3–7]. When a nontrivial topography at the contact area is assumed, a contact situation of partial slip needs to be introduced, next to the two trivial contact states of contact loss and sliding. In the partial slip state, both stick and slip areas can be simultaneously present at the contact interface, as a result of Coulomb's frictional law. For the implementation into the model, the difficulty of meshing all asperities at the contact faces on a microscopic level is avoided by considering a multiscale approach in which mesoscopic cells are introduced in the mesh. Using this approach in a 1D (normal) loading, the complexity of the stress and displacement fields, along with the contact profile and possible roughness can be fitted into a single relationship between normal displacement and normal load.

The authors of this work, together with others, previously developed a 2D contact model. The description of the contact model follows the Method of Memory Diagrams (MMD) to update the contact loads in a semi-analytical manner, not needing to approach the state of the load through variational means [4,5]. Apart from updating the stress at the level of the contact, the 2D contact model is also capable of calculating the instantaneously generated heat induced by friction at the contact interface [8,9]. Traditional implementations on the calculation of dissipated energy generally start from the assumption of cyclic contact behavior, hence a simple closed hysteretic loop, and calculate the area of the hysteric loop to find the dissipated energy per cycle [10,11]. However, despite the fact that the loading procedure may be monofrequent, internal reflections and nonlinear effects will result in complex contact behavior, creating complicated and/or non-closed, hysteretic areas, instead of a single closed loops. Apart from this, having non-static conditions, such as an evolving crack, fatigue of the material, a changing excitation amplitude or frequency as an influence of the bond between actuator and sample ... will also have an effect on the hysteresis area. Therefore, the instantaneous energy dissipation method has been extended to accommodate the MMD contact model as illustrated in previous work for realistic excitation procedures in 2D case studies [8]. Also a passive excitation will result in a nonperiodic contact behaviour as well, making this method of calculating the dissipated energy also valuable for modelling structural health monitoring scenarios through passive excitations. The 2D simulation model clearly reveals the simultaneous presence of nonlinear elastic wave generation, i.e. the generation of higher harmonics of the excitation frequency at the defect location, along with the thermographic response at the defect and its radiation towards the boundaries.

In the present contribution, we develop and discuss a three dimensional model, based on the aforementioned two dimensional model. We perform a qualitative analysis by comparing the obtained numerical results to results described in the literature in order to validate the capability of the three dimensional model to simulate realistic situations.

2. Materials and Methods

As the current three dimensional model is based on the previous two dimensional model described by the authors of this work, the most important ingredients of the computational model will be briefly recapped [4,5,8]. The model consist of three different modules. The first module describes the elastic wave propagation in a virgin material. The second module captures the contact physics at the defect level. This module accounts for anharmonic and hysteretic effects, describing the nonlinear behavior of the defect's interfaces, which is echoed in both the ultrasound spectrum and in the vibration induced heating. The third module is implemented to calculate the diffusion of thermal energy within the specimen. The full model is built in COMSOL Multiphysics® and uses its internal descriptions for the first and third module. The contact response is described through the Method of Memory Diagrams (MMD) in three dimensions and is linked to the computational model through a MATLAB® interface.

2.1. Contact description

By combining the above contact description with the two modules to solve the wave equation in bulk materials and the heat transfer equation in solids, a consistent model can be built to simulate the nonlinear elastic behavior and the vibrothermal response at the defect's contact faces. These are reflected in the nonlinear spectral components in the frequency spectrum and in the thermograms. The extension of the MMD description in 3D can be retrieved in analogy with the two dimensional case. The MMD contact model represents a semi-analytical method that allows to study the dynamic response of a hysteretic tangential contact in the simultaneous presence of a normal contact loading, respectively describing friction and clapping. The normal (σ) and tangential ($\vec{\tau}$) loads are calculated in each point, given the normal indentation a and tangential displacement $\vec{b}$ at that location. The method accounts for roughness at the internal boundaries of the internal defect, assuming the asperities are convex and axisymmetric, following the Mindlin description on contact mechanics [12] and the reduced elastic principle [13,14]. These assumptions allow to avoid an expensive computational procedure of updating the stress profiles to the current position by introducing analytical functions that need to be iteratively updated, as the contact progresses. As mentioned in the introduction, roughness at the contact interfaces introduces a contact state called partial slip when the tangential load is smaller than the product of the frictional coefficient (μ) and the normal load, i.e. when the Coulomb condition for slipping is not yet met ($|\tau| \leq \mu\sigma$). These microscopic aspereties, which are assumed to be convex and axisymmetric, are locally unified in a general mesoscopic cell (which will be the size of the mesh element in the simulations) and generalized into one single convex axisymmetric profile, which exerts an equivalent load to the opposing face. These equivalent loads result in an identical contact behaviour compared to the original family of asperities. Sub-figure (a) of Figure 1 shows an axisymmetric contact in a state when no tangential displacement is applied, after the center of the contact has been indented over a distance q. Sub-figure (b) represents the status of the contact area obtained by increasing the normal indentation to distance a at the center after which a non-zero tangential displacement is applied. As the contact profile is convex, the outer regions will experience a smaller normal load compared to the interior region. Subsequently, the Coulomb friction criterion will be met in the outer regions ($|\tau| = \mu\sigma$), as the tangential load is the same in the entire contact region. As of this, regions with a radius between s and c will generate friction, whereas the inner contact region (with a radius smaller than s) will remain in place and does not slide, as $|\tau| \leq \mu\sigma$ in this region.

To implement the presence of stick, slip and partial slip into the contact model, the normal and tangential loads acting in each point of a contact need to be determined. This can be done by relating them to the displacements. The load-displacement relationship which accounts for the normal dimension is based on both an empirically [15] and a numerically [16] derived quadratic relationship:

$$\sigma = C \cdot a^2, \tag{1}$$

where C is a material dependent constant and is $3.6 \cdot 10^{21} Pa \cdot m^{-2}$ for aluminium. The tangential interaction occurs through the MMD, where the piece-wise memory vector function $\vec{D}(\alpha)$ plays the central role, containing the memory of the hysteretic contact. This vector function is updated through the current tangential displacement vector $\vec{b}$ and used to calculate the tangential load vector $\vec{\tau}$:

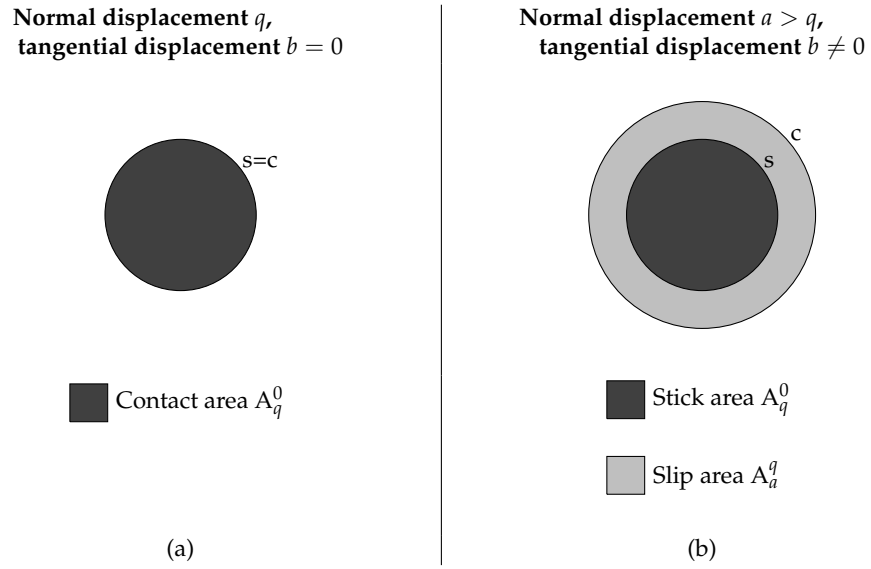

Figure 1. Representation of the 3D axisymmetric contact description, as a generalization of a set of arbitrary contacts, experiencing no tangential displacement (figure a) versus experiencing a tangential displacement (figure b). As a tangential loading is applied to the system, at some contact points, the Coulomb threshold will be met, introducing slip inside the regions with a radius between s and c, where c is the radius of the contact and s is the radius of the stick area. The more central parts of the contact, due to the convex assumption of the contact, will not experience slip, as the Coulomb threshold is not met.

$$\begin{cases} b_x = \theta\mu \int_0^a D_x(\alpha)\, \mathrm{d}\alpha \\ b_y = \theta\mu \int_0^a D_y(\alpha)\, \mathrm{d}\alpha \\ \tau_x = \mu \int_0^a D_x(\alpha) \dfrac{\mathrm{d}\sigma(\alpha)}{\mathrm{d}\alpha}\, d\alpha \\ \tau_y = \mu \int_0^a D_y(\alpha) \dfrac{\mathrm{d}\sigma(\alpha)}{\mathrm{d}\alpha}\, d\alpha \end{cases}, \tag{2}$$

where θ is a material parameter which depends on Poisson's ratio ν [4]. The rules follow the exact same steps as in the 2D case, as explained and illustrated in [4], except that the orthogonal parts of the memory vector function $\vec{D}(\alpha)$, now comprise an area of maximum $\cos\gamma$, respectively $\sin\gamma$, where γ is the angle of the tangential displacement, as they represent orthogonal projections of $\vec{\tau}$. Note that we have assumed isotropy at the moment for the material parameters θ and μ, however, an extension to anisotropic media can be obtained by including the tensor notation of θ and ν.

The energy dissipation in 3D, which determines the amount of energy lost due to friction, can be retrieved in a similar way as in the 2D case, as has been described in Truyaert et al. [9]. This energy is calculated as the inner product of both the tangential load ($\vec{\tau}(\rho)$) and the tangential slip ($\Delta\vec{\Sigma}(\rho)$), inside the slip region,

$$\Delta W = \int_s^c \Big(\vec{\tau}(\rho) \cdot \Delta\vec{\Sigma}(\rho)\Big) 2\pi\rho\, \mathrm{d}\rho. \tag{3}$$

In this expression, the lower and upper boundaries of the integral, s and c, denote the radii of the related circles describing the contact, as depicted in Figure 1. Equation 3 can be conveniently rewritten in terms of the displacement vectors and normal load, which are all inputs of the model, in order to obtain,

$$\Delta W = 2\mu \left[\left|\left| \vec{\Delta b} \right|\right| - \theta \mu \Delta a \right] \cdot \left(\sigma(a) - \sigma(q) + \left. \frac{\mathrm{d}\sigma}{\mathrm{d}a} \right|_{a=q} (q-a) \right), \tag{4}$$

where q corresponds to the normal indentation which would be needed to obtain the non-slipping contact region, as in the right part of Figure 1, and $\left|\left| \vec{\Delta b} \right|\right|$ is the Euclidean norm of the tangential slip displacement vector.

2.2. Computational model

By combining the above described nonlinear and history dependent contact mechanics with the two modules to both solve the wave equation in bulk materials and the heat transfer equation in solids, a consistent model can be built to simulate the nonlinear dynamics of the defect's contact faces. These microscopic and mesoscopic features will be reflected in the macroscopically observable nonlinear spectral components and thermal properties. Simulations performed with the developed model need to be time-dependent in order to correctly capture the generation of the nonlinear effects.

The time stepping procedure, of which a flowchart is present in Figure 2, is as follows:

(a) *Computation of displacements and temperature distribution*
Starting from the local normal and tangential stresses (σ and $\vec{\tau}$), the Structural Mechanics module of COMSOL® calculates the displacements within the entire domain at each time instance t of the procedure. The local normal and tangential displacements (u_n and $\vec{u_t}$) on the contact interface are stored as output of the COMSOL® module, and used as an input for the displacement driven MMD module which is implemented in MATLAB® in the next calculation step (see (b)). Simultaneously, the heat diffusion problem in response to an internal boundary heat source at the contacting surfaces is solved through the Heat Transfer module of COMSOL®, updating the temperature distribution in the entire computational region. In contrast to the contact module which is only addressed for the defect specific nodes, the PDE's for structural mechanics and thermal diffusion are constantly updating all properties in the whole computational region.

(b) *Computation of contact stresses and energy losses*
During this intermediate step, the parameters at the contact interface are updated. The displacement-driven MMD module for the nonlinear and history dependent contact dynamics, implemented in MATLAB®, calculates the new stress parameters at the integration points on the contact interface. Simultaneously, the friction-induced energy loss is calculated for each of these points. The calculated stress values and energy losses are then returned to COMSOL® in order to update the mechanical (i.e. internal thin elastic layer) and thermal (i.e. internal heat source) boundary conditions at the contact interface in respectively the Structural Mechanics and Heat Transfer modules. In this step, only the boundary conditions at the defect interface are updated.

(c) *Repeated calculations*
Steps (a) and (b) are repeated for the next time instance $t + \Delta t$, continuously updating the entire computational region first and then the boundary conditions on the crack. This goes on until the desired calculation time is reached ($t = t_{\text{end}}$).

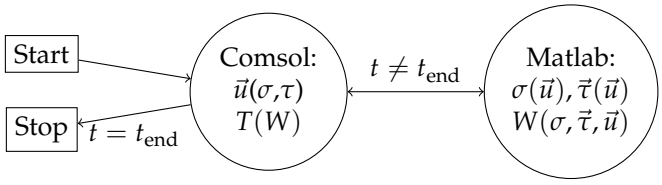

Figure 2. Small flowchart of the computational procedure where the locations of the updates of parameters related to the contact description are highlighted.

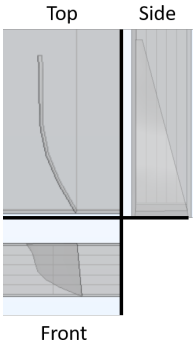

Figure 3. Geometry of the more complex cut.

Both the structural mechanics and thermal module are solved using an appropriate mesh, with its corresponding discretizations and shape functions to the order of the chosen mesh, depending on the given problem. The PDE's for these two modules are solved based on their corresponding mesh, but can communicate a common parameter to each other. In this model, the common parameters (the stresses) are calculated in the description of the contact mechanics through an external MATLAB® script and are fed into both COMSOL® modules, adapted to the appropriate mesh of the module. To qualitatively illustrate the simulation procedure and results, a model consisting of a rectangular block of aluminum of dimension 18 cm-by-10 cm-by-1 cm in x, y and z direction will be considered. On the largest surface of the block, at $z = 0$ m and centered about $x = 0.05$ m and $y = 0.05$ m, a circular zone with a diameter of 1 cm acts as a transducer, exerting a normal displacement in the form of a continuous sinusoidal wave of frequency 70 kHz, with an amplitude of 100 nm. Two different defects are studied. A first synthetic 2D defect in the form of a zero thickness cut is considered located at $x = 15$ cm. The cut is oriented perpendicular to the surface, 3.3 cm deep and runs through the full 1 cm depth of the sample. A second zero thickness defect has a more complex shape, where the defect is open at the front and top side of the sample, while the geometry of the defect is closed through the material. The defect is curved in all three dimensions, runs to the same depth of 3.3 cm depth and the opening at the front side is located at the same place of the first defect. A normal prestress is applied at the defect interface for both studied defects, to increase the time spent in contact, allowing for a larger amount of time where the defect experiences friction instead of clapping. The geometry of both these defects are taken as such to test either a planar cut through the whole sample and a more complex defect which does not run through the whole sample and is curved. The areas around both defects is meshed denser than the other region of the sample. The meshdensity in the healty region of the sample is meshed at 12 elements for each wavelength, whereas the denser region consists of 84 elements for each wavelength. Not only is this area denser to propagate the higher harmonics generated by the clapping and friction of the defect, it is also needed to obtain a stable contact description. All meshelements are quadratic.

3. Results

First, the planar defect will be discussed, after which the more complex geometry is treated. These two different defects are studied in order to have a benchmark for the model (planar defect), which is used to study the numerical stability and performance of the model. The second defect is introduced in order to observe the results of a more realistic defect.

3.1. Planar defect

Figure 4 displays the frequency spectrum of the normal displacement, u_z, at a point on the x-y plane near the planar defect region. It can be clearly seen that higher

harmonics of the excitation frequency are present in the response signal. To ensure that these harmonics directly originate from the defect, the amplitudes at the fundamental frequency and its higher harmonics were examined on the surface of the sample and their distribution is visualized in Figure 5 for the displacement tangential to the defect and in Figure 6 for the displacement in the normal direction to the defect. The results reveal a concentration of the magnitudes of the second and third harmonic in the neighbourhood of the defect and confirm that the origin of these generated frequencies is to be attributed to the interaction of its interfaces: friction (Figure 5) and clapping (Figure 6). From Figures 5 and 6a, b and c it can be concluded that the harmonics are predominantly generated near the tip of the defect, the reason being that the region of the crack tip experiences more stress, compared to the open end of the crack. This is in agreement with experimental observations reported in previous research studies [17].

Apart from the acoustic spectrum, the multiphysics model also allows to produce a map of the thermal response as an output to study. It is expected that the temperature increases as a result of energy dissipated from friction at the defect's interface. Figure 7 displays the temperature increase on the planar surface of the defect (i.e. the partial part of the y-z plane at $x = 0.15$ m, covering only the defected area and no healty material). Again, the crack tip reveals the highest temperature increases. In addition, some smaller

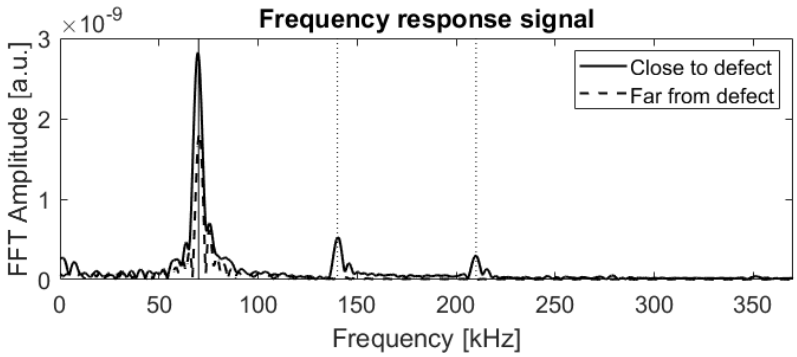

Figure 4. Generation of higher harmonics of the applied frequency, as a result of the friction and clapping of the interfaces of a zero-thickness, planar cut.

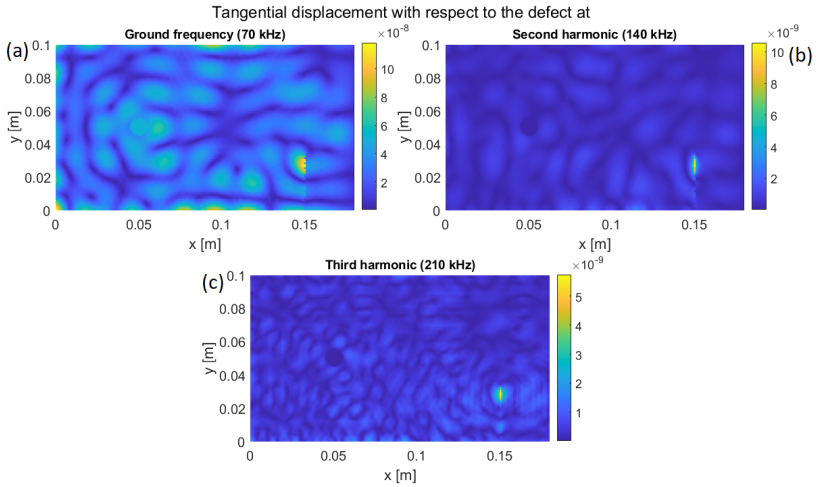

Figure 5. Source of the harmonics of the excitation frequency in a rectangular aluminum block containing a vertical cut at $x = 0.15$ m extending between $y = 0$ m and $y = 0.033$ m. Figure 4a displays the amplitude of the tangential displacement, with relation to the defect, at each location on the surface ($z = 0$ m), calculated by selecting the Fourier transform magnitude at the excitation frequency. Figures 4b and 4c shows the magnitudes of the same signals for the second and the third harmonic respectively.

temperature effect is present near the open edge of the crack. Within the small total simulation time, the temperature distribution is only affected close to the defect's region, as the timescale of the overall thermal response is much larger compared to the acoustic timescale and the timescale of the contact physics. To illustrate this, Figure 8 shows the region of the front surface ($z = 0$ m near the defect, revealing only a thin dissipation zone of the generated heat through the sample. Following Equation 4, temperature increases can be achieved as a result of either a relative large displacement or/and a large stress. The region near the crack tip experiences a large amount of friction, as the higher harmonics are originating from that location, and therefore also temperature will increase from this local heat source. At the crack tip itself however, the asperities of the rough surfaces will be locked, making it unable to displace them and to experience rubbing. Therefore, heating as a result of friction does not take place at the very tip of the defect itself, but only near that area. In addition, the part of the defect that opens up near the free side of the sample also appears to engender an increase of the local temperature and of its surrounding. The component from Equation 4 responsible for this is the relative tangential displacement, as this part of the defect can move more freely.

3.2. Defect with a complex geometry

Again, the amplitudes at the fundamental frequency and its higher harmonics were examined on the surface of the sample and their distribution is visualized in Figure 9 for the displacement tangential to the defect and in Figure 10 for the displacement in the normal direction to the defect. The results reveal a concentration of the magnitudes of the second and third harmonic in the neighbourhood of the defect and confirm that the origin of these generated frequencies is to be attributed to the interaction of its interfaces: friction (Figure 9) and clapping (Figure 10). Friction is more present at the closed part of the defect, whereas clapping is more present at the open part, as is retrieved from both figures. From Figures 9 and 10a, b and c it can be concluded that the harmonics are generated along the length of the defect, the reason being that the region of the crack tip experiences more stress, compared to the open end of the crack, but the open end experiences more movement compared to the closed part. This is in agreement with experimental observations reported in previous research studies [17].

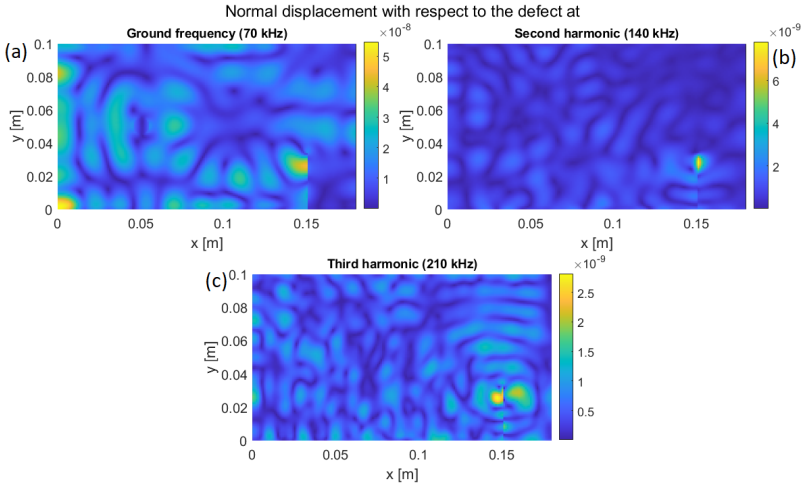

Figure 6. Source of the harmonics of the excitation frequency in a rectangular aluminum block containing a vertical cut at $x = 0.15$ m extending between $y = 0$ m and $y = 0.033$ m. Figure 5a displays the amplitude of the normal displacement, with relation to the defect, at each location on the surface ($z = 0$ m), calculated by selecting the Fourier transform magnitude at the excitation frequency. Figures 5b and 5c shows the magnitudes of the same signals for the second and the third harmonic respectively.

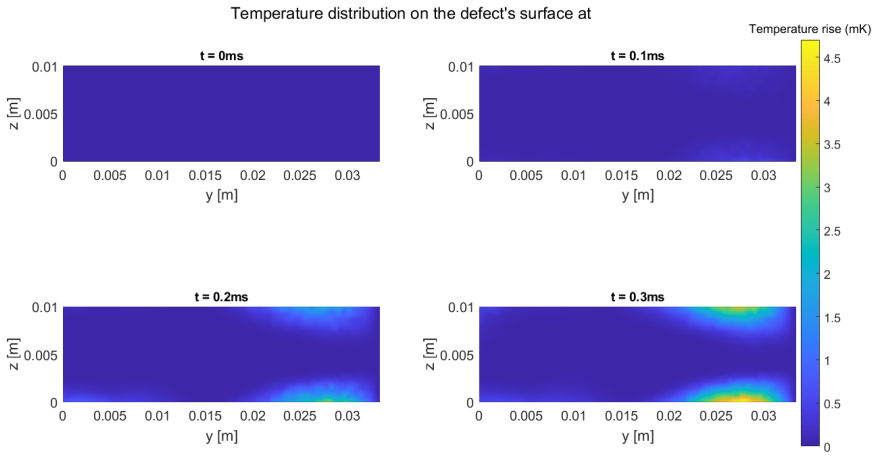

Figure 7. Temperature increase at the defect's surface (partial y-z plane at $x = 0.15$ m over 4 time instances, covering the full defected area without any undamaged part of the sample. The highest temperature increase occurs at surfaces $z = 0$ m and $z = 0.1$ m near the crack tip ($y = 0.033$ m) with some smaller temperature increase also being present at the open edge of the crack.

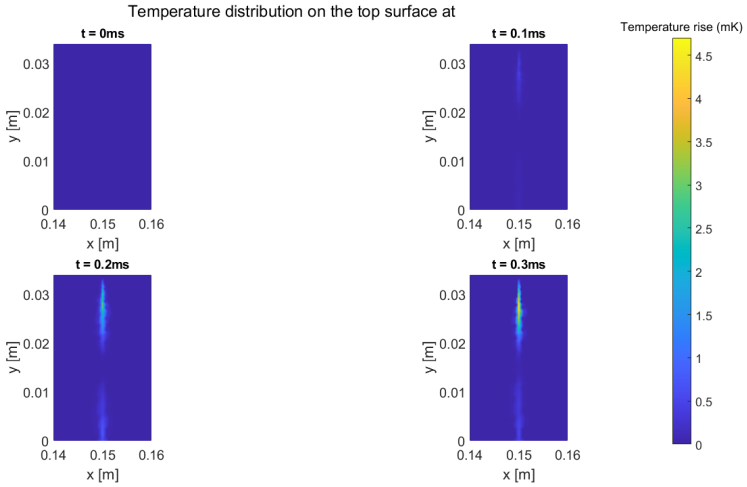

Figure 8. Thermal view from the surface ($z = 0$) of the specimen zoomed in on the region of the defect, showing that the increase in temperature is highest at the edges (tip and open end of the cut) and increases over time.

Apart from the acoustic spectrum, the multiphysics model also allows to produce a map of the thermal response as an output to study. It is expected that the temperature increases as a result of energy dissipated from friction at the defect's interface. Within the small total simulation time, the temperature distribution is only affected close to the defect's region, as the timescale of the overall thermal response is much larger compared to the acoustic timescale and the timescale of the contact physics. To illustrate this, Figure 11 shows the region of the front surface ($z = 0$ m near the defect, revealing only a thin dissipation zone of the generated heat through the sample. Following Equation 4, temperature increases can be achieved as a result of either a relative large displacement

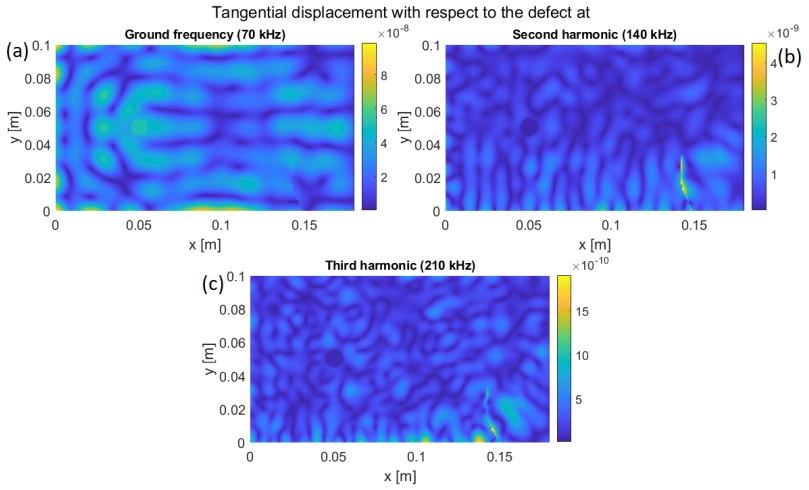

Figure 9. Source of the harmonics of the excitation frequency in a rectangular aluminum block containing a vertical cut at $x = 0.15$ m extending between $y = 0$ m and $y = 0.033$ m. Figure 8a displays the amplitude of the tangential displacement, with relation to the defect, at each location on the surface ($z = 0$ m), calculated by selecting the Fourier transform magnitude at the excitation frequency. Figures 8b and 8c shows the magnitudes of the same signals for the second and the third harmonic respectively.

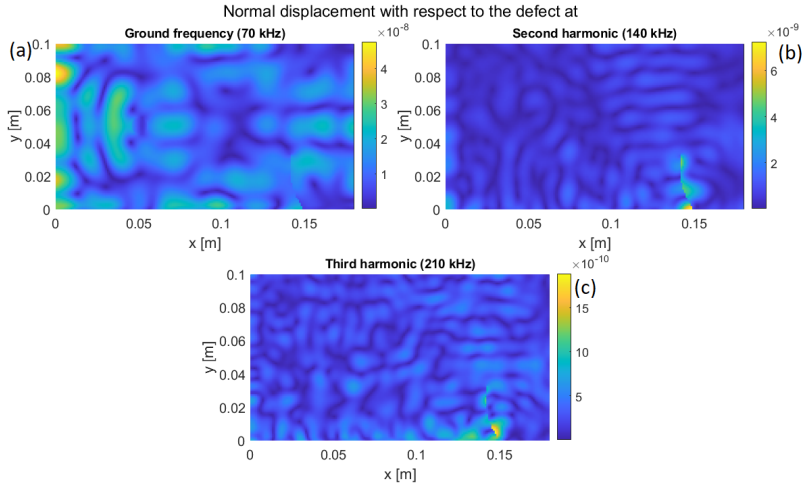

Figure 10. Source of the harmonics of the excitation frequency in a rectangular aluminum block containing a vertical cut at $x = 0.15$ m extending between $y = 0$ m and $y = 0.033$ m. Figure 9a displays the amplitude of the normal displacement, with relation to the defect, at each location on the surface ($z = 0$ m), calculated by selecting the Fourier transform magnitude at the excitation frequency. Figures 9b and 9c shows the magnitudes of the same signals for the second and the third harmonic respectively.

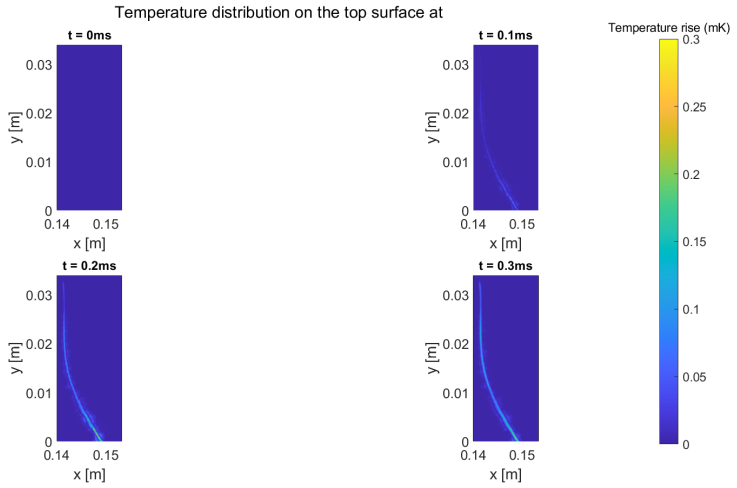

Figure 11. Thermal view from the surface ($z = 0$) of the specimen zoomed in on the region of the defect, showing that the increase in temperature is highest at the edges (tip and open end of the cut) and increases over time.

or/and a large stress. In addition, the part of the defect that opens up near the free side of the sample also appears to engender an increase of the local temperature and of its surrounding. The component from Equation 4 responsible for this is the relative tangential displacement, as this part of the defect can move more freely.

4. Discussion and conclusion

The results of the above qualitative study confirm that the presence of higher harmonics of the excitation frequency is related to the nonlinear behaviour of the defect when it experiences friction and clapping as a result from an acoustic excitation [18–20]. The appearance of a rather large defect (3.3 cm-by-1 cm) can be revealed through the mapping of these nonlinearities in the acoustic spectrum, as these harmonics are originating from the defect, cfr. Figure 5, 6, 9 and 10 [17,21,22]. In addition, the zone of the surface breaking crack that activates these higher harmonics is similar to literature reportings. For instance, Fierro at al. performed experiments on a fatigue surface breaking crack in an aluminium plate and demonstrated that the zones that generated the second harmonic were located near the crack tip [23].

With respect to the thermal response of a dynamical action, Renshaw et al. reported that heating due to dissipation of energy when surfaces experience friction is one of the most significant heating mechanisms during vibrothermography [24]. Rizi et al. developed a phenomenological 3D model to describe the energy dissipated by friction [25]. In both works, the authors communicated that the temperature primarily increases in a region close to the crack tip, where the aspereties are not locked, far more than compared to the crack region near the open part of the specimen or the crack tip itself. These findings were also confirmed in the above mentioned study of Fierro et al. [23].

Analyzing the results obtained with our computational model, it can this be concluded that qualitatively, the presently developped 3D model successfully accounts for the generation of higher harmonics and the origin of heat within both a planar defect and a more complex defect at locations that are in agreement with pioneering reports found in literature, handling both 2D computational models and experiments. Even though the input parameters of the model were not specifically tuned to match a real experiment, the actual temperature increases lay within the expected range. More quantitative results can be obtained on a case by case basis. Currently, the main drawback of the simulation tool is that the three dimensional computational model requires a lot of computational time. For instance, for the specific model discussed here, it took three days to run the 0.3 ms simulation on a desktop.

In the future, we will address more quantitative studies of the developed model, including anisotropic materials, and investigate adaptations to reduce the computational time of the model to acceptable execution times.

Author Contributions: Conceptualization, K.T., V.A. and K.VDA; methodology, K.T. and V.A.; software, K.T.; validation, K.T.; formal analysis, K.T.; investigation, K.T.; resources, K.T. and K.VDA; data curation, K.T.; writing—original draft preparation, K.T.; writing—review and editing, K.VDA.; visualization, K.T.; supervision, K.VDA.; project administration, K.VDA.; funding acquisition, K.VDA and V.A. All authors have read and agreed to the published version of the manuscript.

Funding: The research leading to these results has gratefully received funding from Internal Funds KU Leuven (C24/15/021) and joint doctorate financing by I-SITE ULNE and KU Leuven. One of authors (Vladislav Aleshin) is also grateful to the Tomsk State University competitiveness improvement program.

Conflicts of Interest: The authors declare no conflict of interest.

References

1. Delrue, S.; Van Den Abeele, K. Three-dimensional finite element simulation of closed delaminations in composite materials. *Ultrasonics* **2012**, *52* 315-–324
2. Blanloeuil, P.; Meziane, A.; Bacon, C. Numerical study of nonlinear interaction between a crack and elastic waves under an oblique incidence. *Wave Motion* **2014**, *51* 425—437
3. Plum, R.; Ummenhofer, T. Structural-thermal finite element simulation of vibrothermography applied to cracked steel plates. *Quant. Infrared Thermogr. J.* **2011**, *8* 201-–220
4. Aleshin, V.V.; Delrue, S.; Trifonov, A.; Bou Matar, O.; Van Den Abeele, K. Two dimensional modeling of elastic wave propagation in solids containing cracks with rough surfaces and friction - Part I: Theoretical background. *Ultrasonics* **2018**, *82* 11–18.
5. Delrue, S.; Aleshin, V.V.; Truyaert, K; Bou Matar, O.; Van Den Abeele, K. Two dimensional modeling of elastic wave propagation in solids containing cracks with rough surfaces and friction – Part II: Numerical implementation. *Ultrasonics* **2018**, *82* 19–30.
6. Wang, D.; De Boer, G.; Neville, A.; Ghanbarzadeh, A. A new numerical model for investigating the effect of surface roughness on the stick and slip of contacting surfaces with identical materials. *Tribology International* **2021**, *159* 106947
7. Bonari, J.; Paggi, M.; Reinoso, J. A framework for the analysis of fully coupled normal and tangential contact problems with complex interfaces. *Finite Elements in Analysis and Design* **2021**, *196* 103605
8. Truyaert, K.; Aleshin, V.V.; Delrue, S.; Van Den Abeele K. A Multiscale Numerical Model for Structures with Internal Frictional Contacts. In *Proceedings of the 1st International Conference on Numerical Modelling in Engineering Volume 2: Numerical Modelling in Mechanical and Materials Engineering*. Springer, Singapore, 2019, pp. 77-–89.
9. Truyaert, K.; Aleshin, V.; Van Den Abeele, K.; Delrue, S. Theoretical calculation of the instantaneous friction-induced energy losses in arbitrarily excited axisymmetric mechanical contact systems. *Int. J. Solids Struct.* **2019**, *158*, 268–276.
10. Barber, J.; Davies, M.; Hills, D. Frictional elastic contact with periodic loading. *Int. J. Solids Struct.* **2011**, *48* 2041—2047
11. Putignano, C.; Ciavarella, M.; Barber, J. Frictional energy dissipation in contact of nominally flat rough surfaces under harmonically varying loads. *J. Mech. Phys. Solids* **2011**, *59* 2442-–2454
12. Mindlin, R.; Deresiewicz, H. Elastic spheres in contact under varying oblique forces. *J. Appl. Mech.* **1953**, *20* 327—344
13. Jäger, J. Axi-symmetric bodies of equal material in contact under torsion or shift. *Archive of Applied Mechanics* **1995**, *65(7)* 478–487
14. Ciavarella, M. The generalized Cattaneo partial slip plane contact problem. I—Theory. *International Journal of solids and structures* **1998**, *35(18)* 2349–2362
15. Biwa, S.; Nakajima, S.; Ohno, N. On the acoustic nonlinearity of solid-solid contact with pressure-dependent interface stiffness. *J. Appl. Mech.*, **2004**, *71.4* 508–515
16. Yuan, M.; Lee, T.; Kang, T.; Zhang, J.; Song, S. J.; Kim, H. J. Absolute measurement of ultrasonic non-linearity parameter at contact interface. *Nondestructive Testing and Evaluation* **2015**, *30(4)* 356–372
17. Ulrich, T. J.; Sutin, A.M.; Guyer, R.A.; Johnson, P.A. Time reversal and non-linear elastic wave spectroscopy (TR NEWS) techniques. *International Journal of Non-linear Mechanics* **2008**, *43* 209–216
18. Van Den Abeele, K. A.; Johnson, P. A.; Sutin, A. Nonlinear elastic wave spectroscopy (NEWS) techniques to discern material damage, part I: nonlinear wave modulation spectroscopy (NWMS). *Journal of Research in Nondestructive Evaluation* **2000**, *12(1)* 17–30.
19. Yuan, M.; Zhang, J.; Song, S. J.; Kim, H. J. Numerical simulation of Rayleigh wave interaction with surface closed cracks under external pressure. *Wave Motion* **2015**, *57* 143–153.
20. Delrue, S.; Tabatabaeipour, M.; Hettler, J.; Van Den Abeele, K. Applying a nonlinear, pitch-catch, ultrasonic technique for the detection of kissing bonds in friction stir welds. *Ultrasonics* **2016**, *68* 71–79.
21. Solodov, I.; Rahammer, M.; Derusova, D.; Busse, G. Highly-efficient and noncontact vibro-thermography via local defect resonance. *Quantitative InfraRed Thermography Journal* **2015**, *12(1)* 98-111.

22. Solodov, I.; Bai, J.; Bekgulyan, S.; Busse, G. A local defect resonance to enhance acoustic wave-defect interaction in ultrasonic nondestructive evaluation. *Applied Physics Letters* **2011**, *99(21)* 211911.
23. Fierro, G. P. M.; Ginzburg, D.; Ciampa, F.; Meo, M. Nonlinear ultrasonic stimulated thermography for damage assessment in isotropic fatigued structures. *Journal of Sound and Vibration* **2017**, *404* 102–115.
24. Renshaw, J.; Chen, J. C.; Holland, S. D.; Thompson, R. B. The sources of heat generation in vibrothermography. *NDT& E International*, **2011**, *44(8)* 736–739.
25. Rizi, A. S.; Hedayatrasa, S.; Maldague, X.; Vukhanh, T. FEM modeling of ultrasonic vibrothermography of a damaged plate and qualitative study of heating mechanisms. *Infrared Physics & Technology* **2013**, *61* 101–110.